Post-fire collapse assessment of the Bank Buildings (Belfast, UK) masonry façade via discrete element macro-analysis

Daniele Malomo, Ph.D. [1], Matthew J. DeJong, Ph.D. [2]

[1] Assistant Professor, Department of Civil Engineering, McGill University, 817 Sherbrooke Street West Montréal, H3A 0C3, Canada; email: daniele.malomo@mcgill.ca (corresponding author)

[2] Associate Professor, University of California, Berkeley, Department of Civil and Environmental Engineering, 760 Davis Hall, Berkeley, CA 94720, United States; email: dejong@berkeley.edu

ABSTRACT

On 28 August 2018, a fire broke out in the Bank Buildings, a five-story heritage construction located in the historic center of Belfast (UK), largely destroying its internal structure and leaving the outer unreinforced masonry (URM) walls free-standing. Of particular concern was the structural integrity of the East URM façade, whose cast-iron supporting system was lost in the fire. To assist the initial design of preventive public safety measures and investigate potential consequences of both local and global failures in a reduced timeframe, a simplified discrete element macro-model was developed to simulate various collapse scenarios. In this work, the adopted assumptions and modeling strategies are presented and discussed, including the selection of material properties, damping scheme, and simplified discretization. Predicted failure modes, debris distributions, magnitudes and directions of impact velocities are also compared, and main differences discussed and scrutinized. This practical and innovative application of discrete macro models enabled us to obtain reasonable results - not readily attainable using different analysis approaches - in a timely manner and provide solutions in a critical situation. Such novel employment of discrete element models - previously mostly confined to small-scale research problems - opens new structural simulation opportunities, challenges and research questions and, as such, might be of interest to both applied researchers and structural engineering professionals.

1. INTRODUCTION

Heritage unreinforced masonry (URM) constructions often consist of unique, complex and vulnerable architectural systems. Their structural integrity is particularly sensitive to aging (Ghiassi and Lourenço 2018; Cavalagli et al. 2019), environmental factors (D'Ayala and Aktas 2016), natural (Leite et al. 2013) and manmade (Giardina et al. 2015) hazards, which unavoidably increase the risk of local and global collapse. As comprehensively described in e.g. D'Altri et al. (2020), several modeling approaches of varying degrees of complexity are available for reproducing numerically the structural behavior of URM assemblies. Simplified methods, e.g. those based on story mechanisms (Tomaževič 1987), equivalent single-degree-of-freedom (Abo-El-Ezz et al. 2013; Vamvatsikos and Pantazopoulou 2016) and frame (Penna et al. 2014; Sangirardi et al. 2019) models, have been widely used over the years to study the in-plane-governed response of URM heritage structures, ranging from isolated masonry towers (Valente and Milani 2016) to multiple dynamically-interacting adjacent buildings (Battaglia et al. 2021). Despite the possibility of detailed simulation of damage propagation, including out-of-plane (OOP) effects (particularly relevant for historic structures and typically neglected using simplified techniques), offered by more sophisticated continuum numerical solutions implemented in Finite Element Method (FEM) codes (Ciocci et al. 2018; Saloustros et al. 2019; Lourenço and Silva 2020), the explicit representation of collapse mechanisms still represent an open challenge from a computational viewpoint (Grunwald et al. 2018). For this reason, despite their inability to provide details on separation, re-contact and collision phenomena among produced debris, fast analytical models based on e.g. limit analysis (Block et al. 2006) and force-moment equilibrium macro-blocks (Casapulla et al. 2021) are often the preferred choice by practitioners and applied researchers. A potential numerical modelling solution is the use of discontinuum-based approaches, originally conceived for solving rock mechanics problems (Cundall 1971) and subsequently adapted to the large-displacement analysis of engineering structures (Kawai 1978; Meguro and Hakuno 1994). In this framework, naturally suitable for collapse analysis, each masonry unit can be modeled separately as either a rigid or deformable block, while joint failure occurs along zero-thickness nonlinear spring interfaces. Various successful applications of the Distinct Element Method (DEM), Rigid Body and Spring (RBSM) and hybrid FEM/DEM models are indeed available in current literature, covering the collapse modeling of masonry arches (De Lorenzis et al. 2007; Baraldi et al. 2019), vaults (DeJong et al. 2015; McInerney and DeJong 2015; Masi et al. 2020; Dell'Endice et al. 2021), isolated wall components (Casolo 2017; Gonen et al. 2021), and reduced-scale heritage buildings (Çaktı et al. 2016; Portioli 2019). However, despite recent technological advancements and upgrades to these initial schemes (Pantò et al. 2017; Malomo and DeJong 2020; Pulatsu et al. 2020), performing discontinuum analyses of large-scale complex URM systems often entails a prohibitive computational expense, which currently limits applied researchers and engineering professionals from benefiting from the unique capabilities of discrete modeling methods in practical collapse assessment applications. In this work, a macro-scale DEM model was devised to simulate the collapse response and corresponding debris distribution of the then-free-standing East URM façade of the Bank Buildings (Belfast, UK), a five-story heritage construction heavily damaged by a fire in August 2018 (Stewart 2018). Aimed at supporting the preliminary design of preventive public safety measures in the aftermath of the event (Lohmann and McClafferty 2020), we were asked to investigate, in a reduced timeframe, the potential consequences of several numerically-predicted local/global

collapse scenarios entailing failure mechanisms activated at different heights. This problem presents several challenges, some of which are listed below and discussed in more detail throughout the various sections of the paper:

1- As mentioned above, traditional numerical techniques (e.g. FEM) are unsuitable for explicit collapse analysis; to overcome this issue, we opted for using DEM.

2- Despite being capable of reproducing collapses, DEM models are extremely time-consuming; to provide results in a reasonable timeframe, we developed a simplified modeling strategy that involved the macro-scale discretization of building components, rather than the usual brick-by-brick approach.

3- The building was not accessible in the aftermath of the fire and material properties could not be estimated in-situ, while the degree of connection between the façade and return walls was unclear; to address the first issue, we conservatively adopted high URM tensile strength values (deemed to project collapsed debris at larger distances, increasing safety hazard) and code-based material parameters. To account for the presence of the return walls and the unknown conditions of the façade-to-wall connections, we added to our scenario-based study two cases considering simplified boundary conditions, representative of either undamaged/well-interlocked or damaged return walls.

4- DEM models typically exhibit high sensitivity to damping parameters. To investigate potential differences related to their influence, we have performed our analyses considering either zero to stiffness-proportional damping.

The innovative macro-scale DEM strategy presented in this paper represents a novel contribution to the state-of-the-art. To our knowledge, indeed, this is amongst the first attempts to perform full collapse analyses of large-scale URM structures providing impact and debris predictions for supporting real-world emergency operations. In what follows, adopted assumptions are presented and discussed, as well as the proposed simplified modeling framework that enabled plausible numerical results not readily attainable using different computational approaches.

2. BRIEF DESCRIPTION OF THE BANK BUILDINGS

In this section, the main structural characteristics of the Bank Buildings (see **Figure 1**(a)) before and after the 2018 fire are summarized, along with a brief description of the adopted post-event public safety measures deemed relevant from a numerical modeling perspective. Interested readers may refer to (Lohmann and McClafferty 2020) for additional details.

Figure 1 (a) historical photo of the East façade (National Library of Ireland, The Lawrence Photograph Collection - catalogue.nli.ie), 1880-1900, (b) schematic plan of the urban surrounding, (c) during and post-fire photos (Lohmann and McClafferty 2020)

Bank Buildings is an iconic construction located in the historic center of Belfast (UK), listed as an important heritage asset by the Northern Ireland Environment Agency and a recognized local landmark (Graham 2019). Standing on the site of a bank erected in 1787, from which it allegedly takes its name, the Bank Buildings façade involved in this study was constructed around 1895-1900. It has a rectangular footprint (ca. 30x70m, see **Figure 1**(b)) and four main floors (18m total height) plus an additional level featuring two URM chimneys on both sides (approximately 4m high), and a large central clock. These latter components were left in precarious conditions by the fire and, in an effort to mitigate the potential consequence of a collapse, these less stable high-level elements were removed and stored for conservation or replaced; therefore, these elements were not considered in the numerical analysis in the following sections. As reported in Lohmann and McClafferty (2020), from which the technical details on post-fire securing operations were also taken, the structure originally featured cast-iron columns, wrought-iron beams and timber floors, with URM clay brick perimeter walls of variable thickness (from ca. 2m at the ground floor up to 0.8m at the fourth one) covered by stone facings. In 1975, three bombs were detonated inside Bank Buildings starting a fire that extensively damaged the North façade, prompting the addition of an internal partial steel frame.

Due to the August 2018 fire, the internal structure of the building suffered extensive damage (see **Figure 1**(c)), causing the collapse of the timber floors and the original iron frames (the rebuilt steel frame of the North façade remained largely standing but severely damaged by the fire), leaving the URM perimeter walls free-standing. Amongst other preventive public safety measures, protective 4.88m (height) x 4.88m (width) barriers made of stone-ballasted shipping containers were temporarily positioned in a U shape around the front of the East façade. As further discussed in what follows and shown in **Figure 1**(b), to study impact velocities of debris produced by a potential collapse of the façade with the shipping containers, as well as their masses and spatial distribution for each of the failure scenarios considered, the devised numerical model comprised a simplified virtual representation of the surrounding built environment, containers included.

3. SIMPLIFIED DISCRETE MACRO-MODELING STRATEGY

Discontinuum analysis of URM structures is often performed using a micro-modeling approach, where zero-thickness nonlinear interface springs are allotted to joints (or discontinuities) among rigid units to account for brick-mortar deformability (Lourenço and Rots 1997) and faithfully represent masonry texture. Lately, FEM/DEM hybrid approaches have been also developed (Smoljanović et al. 2013), enabling to consider deformable units as well, although further increasing computational cost and the number of needed mechanical parameters. Despite recent attempts to reduce analysis time using either meso (Pulatsu et al. 2020) and macro-scale (Malomo and DeJong 2020) discrete models, required analysis time was still not compatible with the need to carry out multiple simulations of a full-scale façade up to complete collapse. In this work, indeed, time constraints, lack of in-situ experimental data on materials, unknown post-fire structural conditions of the building and inability to have access inside the building for inspections in the aftermath of the fire, called for an even higher degree of idealization. Additionally, because the primary objective was to simulate the debris field and the maximum plausible debris impact with the protective shipping container barriers, a macro-element strategy was deemed appropriate. In order to simulate the inertia and collision effects involved in building collapse simulations, dynamic analyses were performed.

To this end, a simplified DEM model was developed and implemented in the 3DEC commercial software (Itasca Consulting Group Inc. 2018) that involved a macro-discretization at the component level (see **Figure 2**(a)) of the East façade alone (interlocking with return walls was also considered in one of the scenarios, as further discussed later in the next section), subdivided numerically into an assembly of rigid blocks (assumed density 2000 kg/m^3) connected via zero-thickness nonlinear interface springs, where the mechanical properties of the system were lumped.

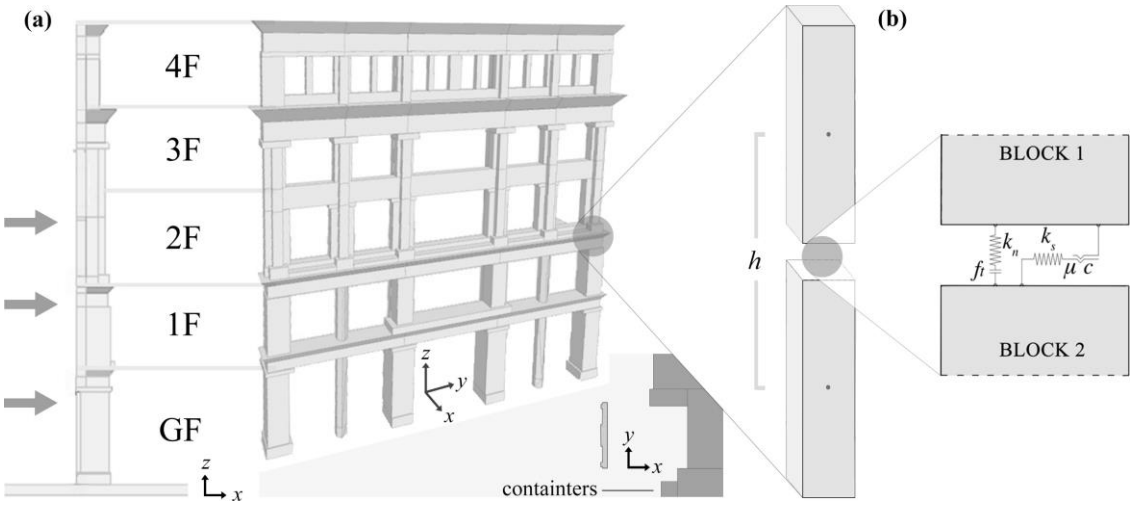

Figure 2 (a) simplified numerical idealization of the East façade and (b) DEM contact modeling among macro-blocks

In the DEM framework, when two rigid blocks, characterized by six degrees of freedom, are in contact, faces are triangulated to create sub-contacts, located at the element vertices, i.e. where the abovementioned springs are created. Interpenetration between adjacent blocks, as in most hard-contact DEM, is regarded as nonphysical and the iterative algorithms originally implemented by Cundall (1988) used to ensure at each step that the mutual distance between centroids is equal or larger than their relative displacements. In the elastic range, the mechanical response of interface springs is governed by k_n and k_s, namely the normal and shear stiffnesses. To account for the deformation of the macro-blocks which are rigid in the model, the continuum stiffness of the masonry was lumped into the joints by defining k_n and k_s as E/h and G/h respectively, with E and G being the Young's and shear moduli (contact area A between blocks is automatically calculated when contact is detected). The Young's modulus E was selected according to the long-term values for masonry suggested by Eurocode 6 (EN 1996-3:2006) and set to 4629 MPa, while G was approximated as G=0.4E=1851 MPa. The parameter h represents the linear distance between the centroids of two adjacent rigid macro-blocks, as shown in **Figure 2**(b); given the variety of different geometries present in the DEM model of the façade, which includes a total of 183 solid elements, the assignment of the various h and corresponding spring stiffness calculations were automated in 3DEC using an iterative C++ function, whose main task was to test each element for contact in the undeformed configuration, extrapolate the mutual distances among centroids, evaluate k_n and k_s values according to the expressions listed above, and assign these values to the 91 joints present in the model. To model shear and tensile failures, a Mohr-Coulomb joint criterion (zero cohesion c, no shear softening; because of the relatively high friction coefficient μ = 0.35, which prevented early relative sliding of blocks, this parameter had negligible effect on results since the predicted collapse response was governed by rocking and thus mostly by tensile strength) with tension cut-off (a joint tensile strength f_t equal to 0.5 MPa was specified; once failure occurs and rigid block separate, contact is lost and so is their mechanical interaction) was employed, while the modeling of crushing damage and dilation phenomena was neglected. The value of f_t, as well as those selected for E and G, should be interpreted as upper bound estimates, also given the typical decay of mechanical characteristics exhibited by brick masonry elements exposed to high temperatures (Russo and Sciarretta 2012; Zhang et al. 2018). Such conservative assumptions were deemed necessary to compensate for the simplified modeling approach proposed and for the high level of uncertainty attached to the limited knowledge of the façade material properties in the immediate aftermath of the fire.

The shipping containers positioned in a U shape around the front of the East façade were explicitly modeled as fixed solid rigid bodies. The containers were included in the model to allow quantification of impact velocities and preliminarily assess the adequacy of the adopted distance between the façade and containers. Because of their asymmetrical distribution (see **Figure 2**) with respect to the façade, a 3D model was employed. Since the objective was to study the nature of a potential collapse, not whether or not collapse would occur, various collapse scenarios (described in more detail in the following) were forced by essentially pushing the façade over. This was done by applying to a number of frictionless rigid elements acting on the top of the loadbearing piers of the considered floor a small velocity (linearly increasing from 0 to 0.1 mm/s in 1 second to avoid energy shocks at contact, and then kept constant until collapse). Zero cohesion and tensile strength were assigned to the interface between these loading blocks and the façade. The implementation of such loading strategy enabled the initially imposed collapse trigger to spontaneously evolve in diverse failure mechanisms, without introducing pre-defined plastic hinges.

4. SCENARIO-BASED COLLAPSE ANALYSIS OVERVIEW

As graphically summarized in **Figure 3**, three main DEM models were developed and then adapted to cover a total of eight collapse scenarios. The first two models, hereinafter referred to as M1 and M2, only differed by the implemented damping scheme. In M1 (**Figure 3**(a)), zero damping was used, meaning that the only source of dynamic relaxation was the energy dissipation induced by the process of crack closure/opening. Recent applications showed that this usually provides adequate results when considering rocking problems (Malomo et al. 2021) and collapse modeling of both reduced (Papantonopoulos et al. 2002) and large-scale (Calvi et al. 2019) systems. Stiffness proportional damping, whose parameters (i.e. stiffness-proportional damping constant β_R=5e-4 and critical frequency f_{crit}=711 Hz at which the system is critically damped) were analytically-evaluated according to the procedure proposed by (DeJong 2009), was used instead in M2 (**Figure 3**(b)) to mitigate spurious bouncing phenomena after impact. The activation of potential collapse mechanisms at each floor (i.e. from the ground floor, GF, to the fourth floor, 4F was initially considered; preliminary results, however, indicated that collapse about the upper floors (i.e. 3F and 4F – it is herein recalled that the fifth floor was removed to reduce the façade height) would not cause impact with the containers, and that, as expected, overturning about the lower floors causes a larger debris runout. Thus, only the more critical collapse scenarios were modeled using M1 and M2, which involve failure at the GF, 1F and 2F. This results in three simulated scenarios for M1 (M1-GF, M1-F1, M1-F2) and as many for M2 (M2-GF, M2-F1, M2-F2).

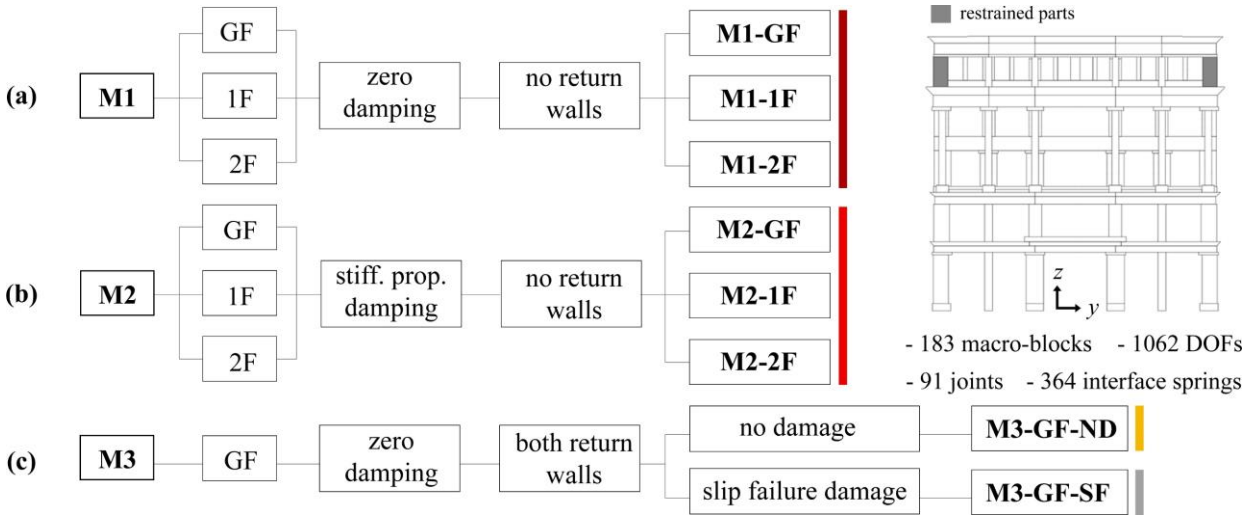

Figure 3 Main features and nomenclature employed for (a) M1, (b) M2 and (c) M3 numerical models

In M1 and M2, the interlocking of the façade ends with the return walls was purposely neglected. This is a conservative assumption, as the return walls could provide very significant resistance to OOP failure, and could cause a partial collapse of the façade, rather than a complete collapse of the entire façade. To provide a rough approximation of how the perpendicular return walls at the ends of the East façade might influence the collapse and simulate this aspect in a simplified way, in M3 (i.e. the last DEM model considered herein, with zero damping) the macro-blocks highlighted in dark grey in **Figure 3**(c) were partially restrained. In this case, only the activation of collapse mechanisms at the GF was considered. This resulted in two additional scenarios, assuming either no damage (ND, which translates in zero velocity along the OOP x-axis direction and zero rotation around the vertical z-axis; this essentially prevented the grey blocks from collapsing while acting as a restraining system for adjacent elements, as if the return wall suffered no damage and only the grey blocks remained attached to them) or slip failure of return walls (SF, with z-velocity=0, z-rotation=0; the grey blocks, in this case, were allowed to slide along the OOP direction x to simulate slip failure to the return walls), named M3-GF-ND and M3-GF-SF respectively. This brings the number of collapse scenarios presented in this work to a total of eight.

5. SUMMARY OF NUMERICAL RESULTS

The main results from the numerical simulations performed according to the scenarios described above are presented in this section, grouped together considering the collapse activation height and summarized in terms of:

(a) collapse mode and macro-blocks impacting the shipping containers

(b) magnitudes of absolute maximum velocities of macro-block centroids along x, y, z (i.e. v_X, v_Y, v_Z) at first impact, magnitudes and directions of the principal velocities of macro-block vertices at first impact (i.e. v_P), masses of impacting parts associated to the maximum velocity values reported (i.e. m_X, m_Y, m_Z, m_P)

(c) final debris distribution

From **Figure 4**, where the imposed displacement was applied at the top of the GF columns, it can be gathered that the introduction of different damping schemes and boundary conditions did have a major effect on the predicted responses. With reference to M1-GF (no damping, GF-triggered collapse, no return walls) and M2-GF (stiffness proportional damping, GF-triggered collapse, no return walls), and despite the similar collapse mode (scan the QR codes to see the videos) and pre/first-impact velocities (it is herein recalled that first-impact velocities were calculated after the first collision, i.e. not considering subsequent contacts), markedly different final debris distributions were simulated. As expected, the final debris configuration obtained using M1-GF reflected the fact that the system was undamped, with no energy loss due to the collisions among elements. While the added damping implemented in M2-GF (which still likely underestimates the actual damping that would occur) yielded more plausible outcomes in this sense, these modeling results still provide only a rough approximation of the actual behavior after impact with the ground. Nevertheless, this simplified approach enables the possibility to evaluate impact with the back of the containers and to estimate the order of magnitude of the macro-block impact velocities. Of interest is also the comparisons shown in **Figure 4** (a) between the different failure mechanisms exhibited by M1-GF, M3-GF-ND (no damping, GF-triggered collapse, undamaged return walls) and M3-GF-SF (no damping, GF-triggered collapse, slip failure of return walls), where the boundary conditions applied to the side elements of 4F significantly influenced the predicted response. Indeed, despite that the collapse trigger was imposed in all the models at the same level (i.e. at the top of the GF columns), the presence of the return walls in M3-GF-ND and M3-GF-SF resulted in a different evolution of the global failure mode, particularly at the upper levels, leaving the GF and 1F still standing after the collapse. However, this also translated into an early separation of some of the 4F

side macro-blocks from the façade during the collapse of M3-GF-ND, which explained the larger v_P value (almost doubled with respect to its M1-GF counterpart) displayed in **Figure 4** (b). Meanwhile, the assumed boundary conditions in M3-GF-SFcaused some debris to fall backwards, i.e. inside the building, thus avoiding the impact with the containers. For both of these last models, macro-blocks started to interact dynamically before impacting the ground, which combined with the lack of damping contributed to an unrealistically-large final debris footprint (see **Figure 4** (c)).

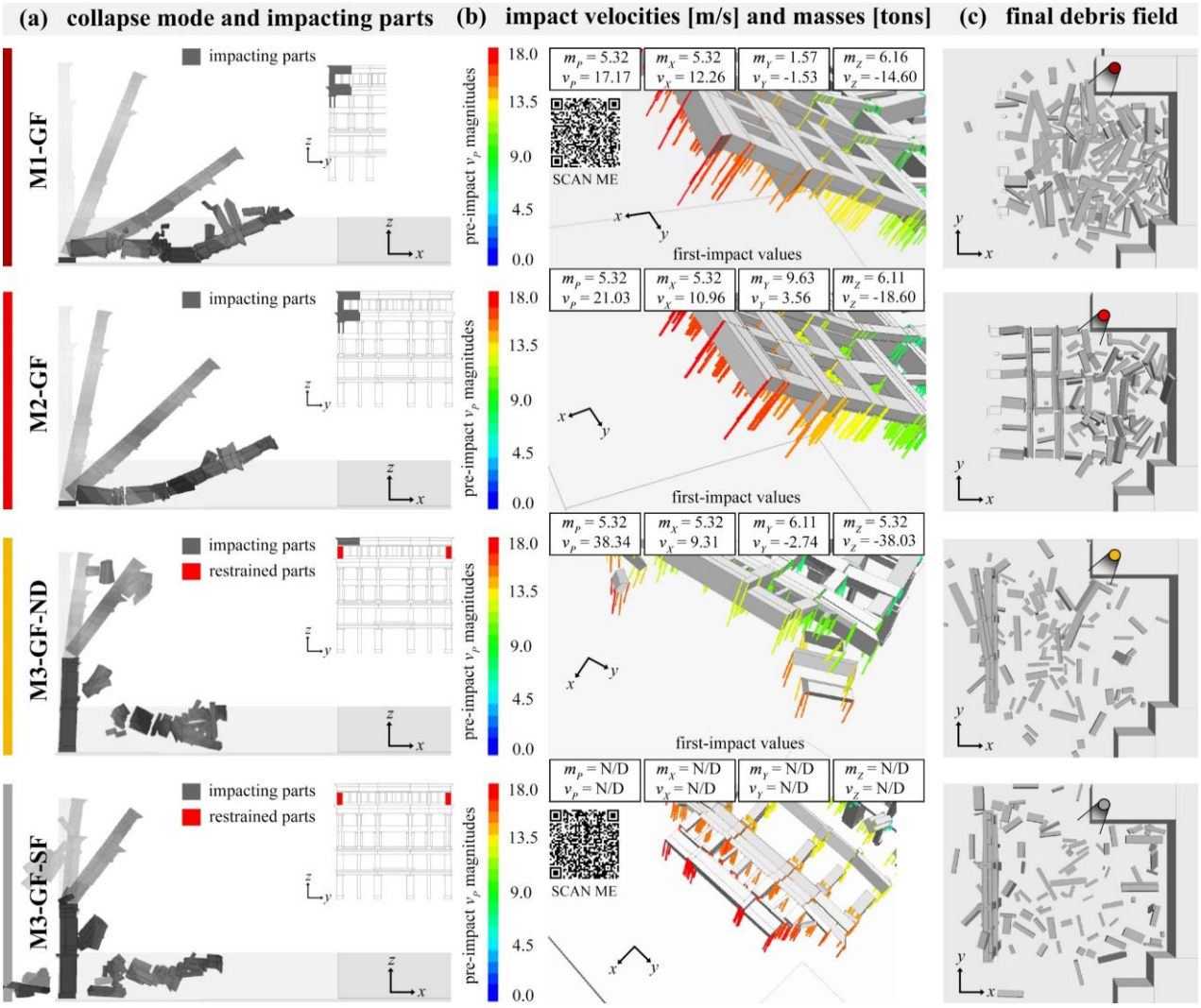

Figure 4 GF-triggered collapses: (a) collapse mode and impacting parts, (b) impact velocities/masses (c) debris field

Analogous failure modes were obtained by M1-F1 (no damping, 1F-triggered collapse, no return walls) and M2-F1 (stiffness proportional damping, 1F-triggered collapse, no return walls), as depicted in **Figure 5**(a), where direct impact with the containers was only detected for only a minor portion of the 4F top left-hand side. As for M3-GF-ND and M3-GF-SF, hinges formed at the bottom of the 2F columns. Despite the larger first-impact velocities of M1-1F (**Figure 5**(b)), only minor differences with M2-F1 are observed in the simulated final debris field (see **Figure 5**(c)).

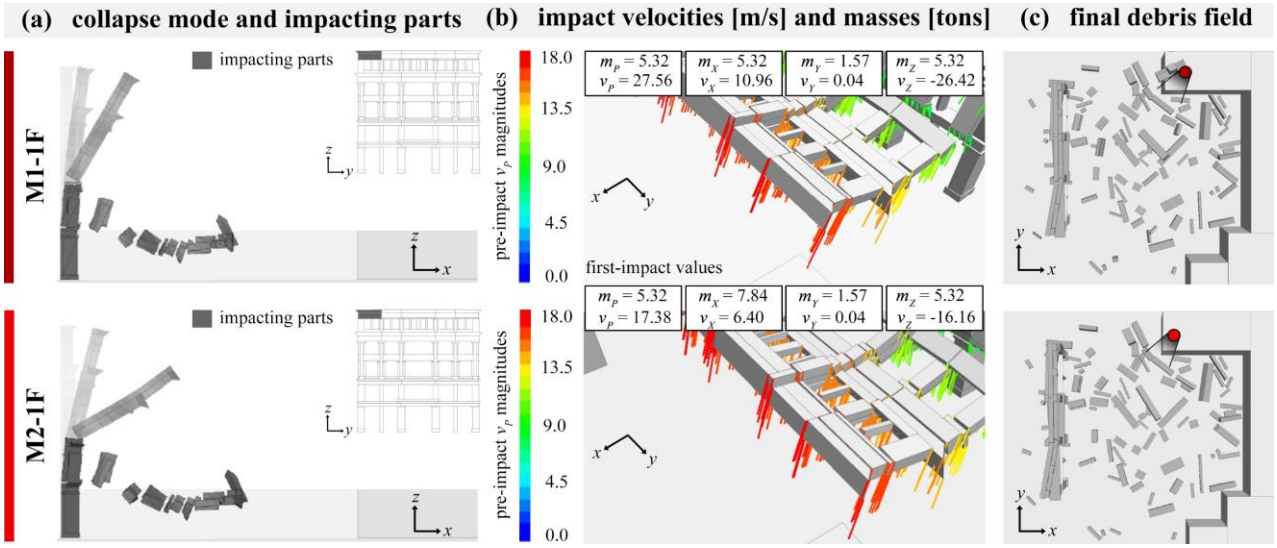

Figure 5 1F-triggered collapses: (a) collapse mode and impacting parts, (b) impact velocities/masses (c) debris field

In M1-2F (no damping, 2F-triggered collapse, no return walls) and M2-2F (stiffness proportional damping, 2F-triggered collapse, no return walls), collapsed macro-blocks only included 2F, 3F and 4F elements, and the macro-blocks impacting the containers were the same as predicted by M1-1F and M2-2F (i.e. the top left-hand side ones, 4F – see **Figure 6**(a)).

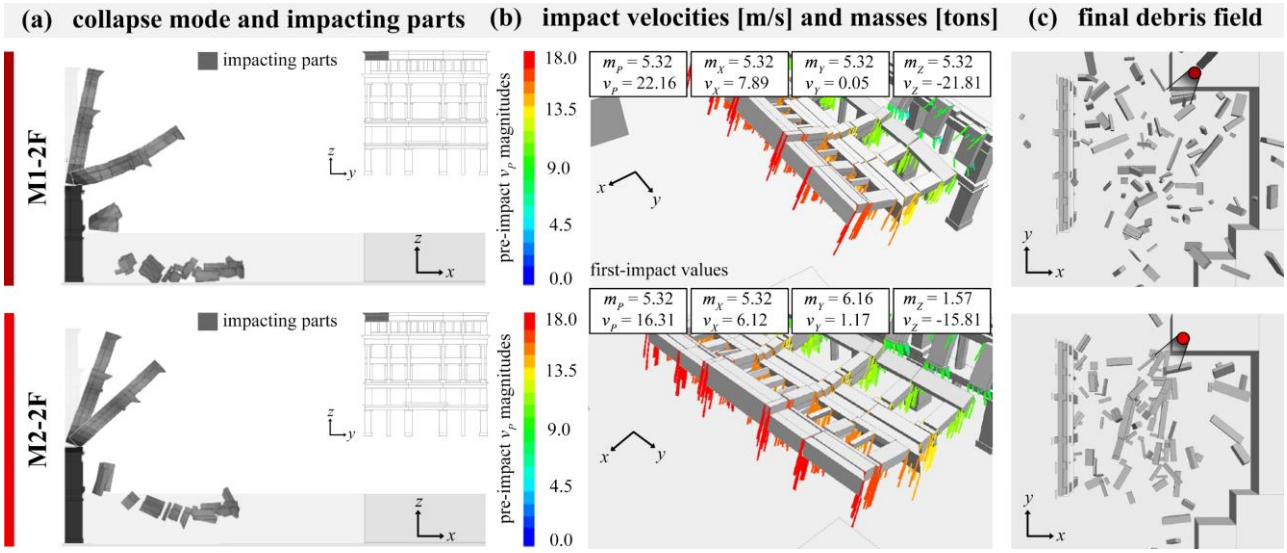

Figure 6 2F-triggered collapses: (a) collapse mode and impacting parts, (b) impact velocities/masses (c) debris field

Pre- and first-impact velocities were also comparable (**Figure 6**(b)), as well as final debris fields. However, in M1-2F, some 4F macro-blocks, after impacting the ground, unrealistically bounced on the top of the containers, as shown in **Figure 6**(c). This latter response was considered a spurious numerical phenomenon, attributable to the lack of damping in the model. In **Figure 7**, a selection of numerically-inferred relevant quantities obtained using different models and assumptions are summarized and compared to each other. The collapsed and first-impacting macro-blocks areas, volumes and principal velocities (i.e. V_c, V_i, A_c, V_i, v_p), displayed below were normalized with respect to the corresponding overall maximum values, for enabling a more effective comparison.

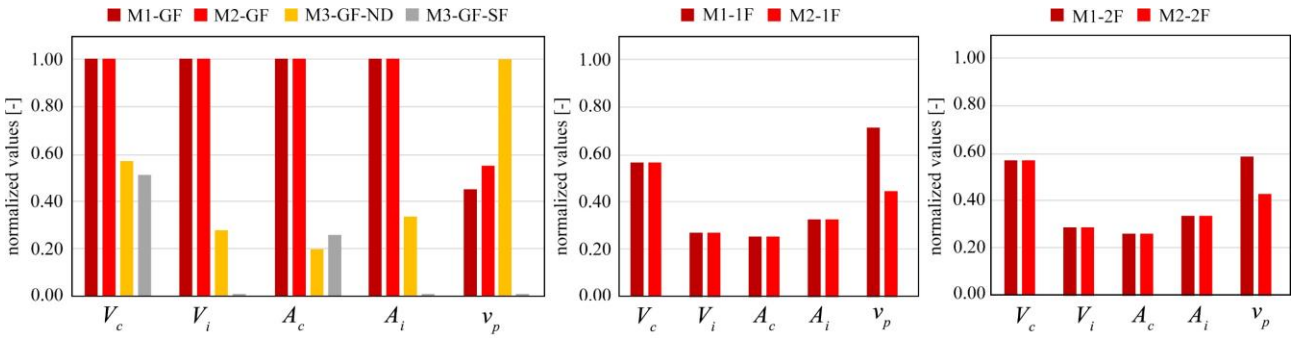

Figure 7 Normalized key-quantities: comparison between the M1, M2 and M3 models

As expected, higher collapsed volumes are associated with GF models, although noticeable differences, not readily predictable prior to the numerical study, were found among M1-M2 and M3. The presence of the return walls in M3 resulted in a shift of the height of the mechanism activation to the upper levels, which left the first three floors standing explaining the fact that V_c values were significantly smaller than M1 (-43%) and M2 (-49%) counterparts. However, the altered boundary conditions of M3-GF-ND caused blocks to interact dynamically before the first external impact, which made the predicted v_p +40% larger than the other simulated values. Of interest is also that no direct impact with containers was predicted by M3-GF-SF, since some upper-level macro-blocks collapsed inside the building. Considerably lower quantities were obtained when considering collapse triggers at 1F and 2F. As per the final debris distributions, no damping models (i.e. M1 and M3) often produced unrealistic footprints due to the fact that no energy was lost during impacts. More plausible debris fields were predicted using M2 models.

For future comparisons, it is worth mentioning that performing a single collapse scenario (up to the point where all the macro-blocks had zero displacements) took approximately 4–5 hours (CPU Intel Core i7 7820x, 64GB DDR4, SSD M2-960-EVO); this time almost doubled in cases where no damping was used. Typically, stiffness damping leads to larger run times, due to the reduced time step; in our analyses, however, the time required for the blocks to reach the equilibrium positions in the undamped case seemed to have governed the computational expense. The average time needed for the modeled façade to reach the ground varied from 1 to 2 hours, which means that most of the relevant data required for the preliminary design of preventive public safety measures (e.g. impact occurrence, velocities, macro-blocks involved in the first collision, etc.) could be obtained in a reasonable timeframe, orders of magnitude smaller if compared with the computational cost entailed by discrete element micro-modeling strategies often used for simulating the dynamic response of URM structures (Galvez et al. 2018).

6. CONCLUSIONS

In this work, the collapse assessment of the East (front) unreinforced masonry (URM) façade of the Bank Buildings, an important five-story heritage construction located in the historic center of Belfast (UK) that was badly damaged by a fire in August 2018, was undertaken to support the design of preventive public safety measures put in place in the aftermath of the event. To use discrete element analysis without prohibitive computational cost in order to deliver plausible results of practical help for decision-makers, and in a critical situation and with only limited time available, a total of eight simplified models were devised. The façade geometry was thus idealized as an assembly of rigid bodies connected via zero-thickness nonlinear springs, where failure occurs and system deformability was concentrated. Code-based values were used for estimating material properties, since no access to the building was possible after the fire. To mitigate the effect of uncertainties, conservative assumptions were adopted and the decrease in mechanical performance of masonry exposed to fire was only partially accounted for numerically. Similarly, only in two of the eight DEM models (i.e. M3-GF-ND and M3-GF-SF), the interlocking of the façade ends with the return walls was considered.

DEM enabled direct simulation of potential failure modes and ensuing debris fields. To simulate potential worst-case scenario collapse scenarios, the assumption of no support from return walls for configurations M1-GF (zero damping) and M2-GF (stiffness-proportional damping) resulted in the largest volume of collapsed elements. Meanwhile, the inclusion of return walls in M3-GF-ND, along with the assumption of zero damping, resulted in maximum values of pre-impact velocity. Although the zero damping case is probably the less realistic option, over which other solutions are generally preferable, we decided to make this further conservative assumption for M1 and M3 models, given the large uncertainties attached to most of the employed numerical parameters. For M3-GF-SD, which included more realistic boundary conditions that accounted for the interlocking with return walls, markedly different responses were obtained with significantly lower first-impacting macro-blocks areas, volumes and principal velocities. It should be mentioned, however, that due to the simplifications introduced in this work, the data discussed above – especially those affected by first-impact phenomena, including computed final debris distributions – must be considered as only rough approximations of actual behavior. Among the other simplifications made, it should be mentioned that neglecting the internal breakage

of macro-blocks might be referred to as an additional source of conservatism, whose quantification would constitute a promising future development. Future comparisons with e.g. real-world collapse field data and/or experimental outcomes, might help to quantify further potential inaccuracies and refine the proposed modeling strategy. Nevertheless, the employed modeling approach enabled the use of discontinuum analysis as a viable option for timely simulation of a very complex and practical structural engineering problem – not readily solvable using other computational solutions – and supported decision-making processes in a critical situation. Other potential applications of such a methodology include e.g. supporting urgent post-disaster restoration interventions (as implemented in various national and international guidelines, see e.g. Coburn and Spence 2002) through the low-cost and prompt estimation of various emergency design alternatives.

ACKNOWLEDGMENTS

The authors would like to acknowledge the support and collaboration of Alessandro Maccioni and the whole Expedition team and thank all the participants and organizations involved in the project, which were undoubtedly presented with a challenging problem in a complex environment. Finally, the authors are grateful to five anonymous reviewers for their insightful suggestions, who significantly contributed to improving the quality of this manuscript.

REFERENCES

Abo-El-Ezz A, Nollet MJ, Nastev M (2013) Seismic fragility assessment of low-rise stone masonry buildings. Earthq Eng Eng Vib 12:87–97. https://doi.org/10.1007/s11803-013-0154-4

Baraldi D, Boscato G, De Carvalho Bello CB, et al (2019) Discrete and finite element models for the analysis of unreinforced and partially reinforced masonry arches. Key Eng Mater 817 KEM:229–235. https://doi.org/10.4028/www.scientific.net/KEM.817.229

Battaglia L, Ferreira TM, Lourenço PB (2021) Seismic fragility assessment of masonry building aggregates: A case study in the old city Centre of Seixal, Portugal. Earthq Eng Struct Dyn 50:1358–1377. https://doi.org/10.1002/eqe.3405

Block P, Ciblac T, Ochsendorf J (2006) Real-time limit analysis of vaulted masonry buildings. Comput Struct 84:1841–1852

Çaktı E, Saygılı Ö, Lemos J V., Oliveira CS (2016) Discrete element modeling of a scaled masonry structure and its validation. Eng Struct 126:224–236. https://doi.org/10.1016/j.engstruct.2016.07.044

Calvi GM, Moratti M, O'Reilly GJ, et al (2019) Once upon a Time in Italy: The Tale of the Morandi Bridge. Struct Eng Int 29:198–217. https://doi.org/10.1080/10168664.2018.1558033

Casapulla C, Argiento LU, Maione A, Speranza E (2021) Upgraded formulations for the onset of local mechanisms in multi-storey masonry buildings using limit analysis. Structures 31:380–394. https://doi.org/10.1016/j.istruc.2020.11.083

Casolo S (2017) A numerical study on the cumulative out-of-plane damage to church masonry façades due to a sequence of strong ground motions. Earthq Eng Struct Dyn 46:2717–2737. https://doi.org/10.1002/eqe.2927

Cavalagli N, Kita A, Castaldo VL, et al (2019) Hierarchical environmental risk mapping of material degradation in historic masonry buildings: An integrated approach considering climate change and structural damage. Constr Build Mater 215:998–1014. https://doi.org/10.1016/j.conbuildmat.2019.04.204

Ciocci MP, Sharma S, Lourenço PB (2018) Engineering simulations of a super-complex cultural heritage building: Ica Cathedral in Peru. Meccanica 53:1931–1958. https://doi.org/10.1007/s11012-017-0720-3

Coburn A, Spence R (2002) Earthquake protection. J. Wiley

Cundall PA (1988) Formulation of a three-dimensional distinct element model-Part I. A scheme to detect and represent contacts in a system composed of many polyhedral blocks. Int J Rock Mech Min Sci 25:107–116. https://doi.org/10.1016/0148-9062(88)92293-0

Cundall PA (1971) A computer model for simulating progressive large-scale movements in blocky rock systems. In: In Proceedings of the Symposium of the International Society of Rock Mechanics. Nancy, France, p No. 8

D'Altri AM, Sarhosis V, Milani G, et al (2020) Modeling Strategies for the Computational Analysis of Unreinforced Masonry Structures: Review and Classification. Arch Comput Methods Eng 27:1153–1185. https://doi.org/10.1007/s11831-019-09351-x

D'Ayala D, Aktas YD (2016) Moisture dynamics in the masonry fabric of historic buildings subjected to wind-driven rain and flooding. Build Environ 104:208–220. https://doi.org/10.1016/j.buildenv.2016.05.015

De Lorenzis L, DeJong MJ, Ochsendorf JA (2007) Failure of masonry arches under impulse base motion. Earthq Eng Struct Dyn 36:2119–2136. https://doi.org/10.1002/eqe.719

DeJong MJ (2009) Seismic Assessment Strategies for Masonry Structures. PhD Thesis, Massachusetts Inst Technol United States

DeJong MJ, Giardina G, Plunkett W, Ochsendorf J (2015) Seismic design of a stone vault. In: In Proceedings of the Society for Earthquake and Civil Engineering Dynamics Conference (SECED). Cambridge, United Kingdom, pp

1–10

Dell'Endice A, Iannuzzo A, DeJong MJ, et al (2021) Modelling imperfections in unreinforced masonry structures: Discrete element simulations and scale model experiments of a pavilion vault. Eng Struct 228:111499. https://doi.org/10.1016/j.engstruct.2020.111499

EN 1996-3:2006 Design of masonry structures - Part 3: Simplified calculation methods for unreinforced masonry structures. Eurocode 6

Galvez F, Giaretton M, Abeling S, et al (2018) Discrete Element modelling of a two-storey unreinforced masonry scaled model. In: 16th European Conference on Earthquake Engineering. Thessaloniki, Greece

Ghiassi B, Lourenço PB (2018) Long-term Performance and Durability of Masonry Structures: Degradation Mechanisms, Health Monitoring and Service Life Design. Woodhead Publishing

Giardina G, Hendriks MAN, Rots JG (2015) Sensitivity study on tunnelling induced damage to a masonry façade. Eng Struct 89:111–129. https://doi.org/10.1016/j.engstruct.2015.01.042

Gonen S, Pulatsu B, Soyoz S, Erdogmus E (2021) Stochastic discontinuum analysis of unreinforced masonry walls: Lateral capacity and performance assessments. Eng Struct 238:112175. https://doi.org/10.1016/j.engstruct.2021.112175

Graham R (2019) The Bank Buildings: The story behind the façade. In: Public Rec. Off. North. Irel. - online Resour. https://www.nidirect.gov.uk/articles/bank-buildings-story-behind-facade. Accessed 12 May 2021

Grunwald C, Khalil AA, Schaufelberger B, et al (2018) Reliability of collapse simulation – Comparing finite and applied element method at different levels. Eng Struct 176:265–278. https://doi.org/10.1016/j.engstruct.2018.08.068

Itasca Consulting Group Inc. (2018) 3DEC – Three Dimensional Distinct Element Code, Ver. 5.20 User's Manual

Kawai T (1978) New discrete models and their application to seismic response analysis of structures. Nucl Eng Des 48:207–229

Leite J, Lourenco PB, Ingham JM (2013) Statistical assessment of damage to churches affected by the 2010-2011 canterbury (New Zealand) earthquake sequence. J Earthq Eng 17:73–97. https://doi.org/10.1080/13632469.2012.713562

Lohmann T, McClafferty J (2020) Bank Buildings, Belfast, UK: Making safe after a fire. Proc Inst Civ Eng Forensic Eng 172:97–106. https://doi.org/10.1680/jfoen.19.00026

Lourenço PB, Rots JG (1997) Multisurface Interface Model for Analysis of Masonry Structures. J Eng Mech 123:660–668. https://doi.org/10.1061/(ASCE)0733-9399(1997)123:7(660)

Lourenço PB, Silva LC (2020) Computational applications in masonry structures: From the meso-scale to the super-large/super-complex. Int J Multiscale Comput Eng 18:1–30. https://doi.org/10.1615/IntJMultCompEng.2020030889

Malomo D, DeJong MJ (2020) A Macro-Distinct Element Model (M-DEM) for simulating the in-plane cyclic behavior of URM structures. Eng Struct 227:111428. https://doi.org/10.1016/j.engstruct.2020.111428

Malomo D, Mehrotra A, DeJong MJ (2021) Distinct element modeling of the dynamic response of a rocking podium tested on a shake table. Earthq Eng Struct Dyn 50:1469–1475. https://doi.org/10.1002/eqe.3404

Masi F, Stefanou I, Maffi-Berthier V, Vannucci P (2020) A Discrete Element Method based-approach for arched masonry structures under blast loads. Eng Struct 216:110721. https://doi.org/10.1016/j.engstruct.2020.110721

McInerney J, DeJong MJ (2015) Discrete Element Modeling of Groin Vault Displacement Capacity. Int J Archit Herit 9:1037–1049. https://doi.org/10.1080/15583058.2014.923953

Meguro K, Hakuno M (1994) Application of the Extended Distinct Element Method for collapse simulation of a double deck bridge. J Struct Eng Eng 10:175–185. https://doi.org/10.2208/jscej.1994.483_17

Pantò B, Cannizzaro F, Caliò I, Lourenço PB (2017) Numerical and experimental validation of a 3D macro-model for the in-plane and out-of-plane behavior of unreinforced masonry walls. Int J Archit Herit 11:946–964

Papantonopoulos C, Psycharis IN, Papastamatiou DY, et al (2002) Numerical prediction of the earthquake response of classical columns using the distinct element method. Earthq Eng Struct Dyn 31:1699–1717. https://doi.org/10.1002/eqe.185

Penna A, Lagomarsino S, Galasco A (2014) A nonlinear macroelement model for the seismic analysis of masonry buildings. Earthq Eng Struct Dyn 43:159–179

Portioli FPA (2019) Rigid block modelling of historic masonry structures using mathematical programming: a unified formulation for non-linear time history, static pushover and limit equilibrium analysis. Bull Earthq Eng 1–29. https://doi.org/10.1007/s10518-019-00722-0

Pulatsu B, Erdogmus E, Lourenço PB, et al (2020) Simulation of the in-plane structural behavior of unreinforced masonry walls and buildings using DEM. Structures 27:2274–2287. https://doi.org/10.1016/j.istruc.2020.08.026

Russo S, Sciarretta F (2012) Experimental and Theoretical Investigation on Masonry after High Temperature Exposure. Exp Mech 52:341–359. https://doi.org/10.1007/s11340-011-9493-0

Saloustros S, Pelà L, Contrafatto FR, et al (2019) Analytical Derivation of Seismic Fragility Curves for Historical Masonry Structures Based on Stochastic Analysis of Uncertain Material Parameters. Int J Archit Herit 13:1142–1164. https://doi.org/10.1080/15583058.2019.1638992

Sangirardi M, Liberatore D, Addessi D (2019) Equivalent Frame Modelling of Masonry Walls Based on Plasticity and Damage. Int J Archit Herit 13:1098–1109. https://doi.org/10.1080/15583058.2019.1645240

Smoljanović H, Živaljić N, Nikolić Ž (2013) A combined finite-discrete element analysis of dry stone masonry structures. Eng Struct 52:89–100. https://doi.org/10.1016/j.engstruct.2013.02.010

Stewart A (2018) NI papers: shock as iconic building burns. BBC News - North. Irel.

Tomaževič M (1987) Dynamic modelling of masonry buildings: storey mechanism model as a simple alternative. Earthq Eng Struct Dyn 15:731–749

Valente M, Milani G (2016) Non-linear dynamic and static analyses on eight historical masonry towers in the North-East of Italy. Eng Struct 114:241–270. https://doi.org/10.1016/j.engstruct.2016.02.004

Vamvatsikos D, Pantazopoulou SJ (2016) Simplified mechanical model to estimate the seismic vulnerability of heritage unreinforced masonry buildings. J Earthq Eng 20:298–325. https://doi.org/10.1080/13632469.2015.1060583

Zhang J, Ma H, Li C, et al (2018) Experimental study on seismic performance of fire-exposed perforated brick masonry wall. Constr Build Mater 180:77–91. https://doi.org/10.1016/j.conbuildmat.2018.05.254